Title

Chemical and Toxicological Properties of Emissions from a Light-Duty Compressed Natural Gas Vehicle Fueled with Renewable Natural Gas

Journal

Environmental Science and Technology, 55(5)

ISSN

0013-936X

Authors

Li, Yin
Xue, Jian
Peppers, Joshua
et al.

Publication Date

2021-03-02

DOI

10.1021/acs.est.0c04962

Peer reviewed

HHS Public Access

Author manuscript

Environ Sci Technol. Author manuscript; available in PMC 2021 July 16.

Published in final edited form as:

Environ Sci Technol. 2021 March 02; 55(5): 2820–2830. doi:10.1021/acs.est.0c04962.

Chemical and Toxicological Properties of Emissions from a Light-Duty Compressed Natural Gas Vehicle Fueled with Renewable Natural Gas

Yin Li, **Jian Xue**

Department of Civil and Environmental Engineering, University of California – Davis, Davis, California 95616, United States

Joshua Peppers

Department of Biological and Agricultural Engineering, University of California – Davis, Davis, California 95616, United States

Norman Y. Kado, **Christoph F.A. Vogel**

Department of Environmental Toxicology and Center for Health and the Environment, University of California – Davis, Davis, California 95616, United States

Christopher P. Alaimo, **Peter G. Green**

Department of Civil and Environmental Engineering, University of California – Davis, Davis, California 95616, United States

Ruihong Zhang, **Bryan M. Jenkins**

Department of Biological and Agricultural Engineering, University of California – Davis, Davis, California 95616, United States

Minji Kim, **Thomas M. Young**, **Michael J. Kleeman**

Corresponding Author: **Michael J. Kleeman** – Department of Civil and Environmental Engineering, University of California – Davis, Davis, California 95616, United States; Phone: 530 752 8386; mjkleeman@ucdavis.edu.

The authors declare no competing financial interest.

Complete contact information is available at: https://pubs.acs.org/10.1021/acs.est.0c04962

Supporting Information

The Supporting Information is available free of charge at https://pubs.acs.org/doi/10.1021/acs.est.0c04962.

Description of biomethane composition analysis; description of engine exhaust toxicity analysis; description of engine exhaust nontarget chemical analysis; description of elastic net regression on exhaust features and toxicity responses; discussion on fuel economy and CO_2 emissions; discussion on carbon monoxide and unburned HCs emissions; discussion on nitrogen oxides, nitrous oxide, and ammonia emissions; and discussion on particulate matter emissions and size distributions. Table S1: Experimentally determined limit of detection (LOD) for different compounds measured by FTIR. Table S2: Experimentally determined LOD for different compounds measured by PTR-MS. Table S3: Concentration (%) of major compounds measured in different fuels. Table S4: Concentration (ppbv) of different sulfur-containing compounds measured in different fuels. Table S5: Concentration (ppbv) of different hydrocarbons measured in different fuels. Table S6: Concentration (%) of major compounds measured in different biomethane streams. Table S7: Concentration (ppbv) of different sulfur-containing compounds measured in different biomethane streams. Table S8: Concentration (ppbv) of different hydrocarbons measured in different biomethane streams. Table S9: PM mass (μg/filter) collected for different toxicity assays. Table S10: Abundance of compounds detected with XAD + GC/MS analysis from different exhaust samples. Figure S1: Speed time trace for the California Unified Cycle. Figure S2: Fuel economy and emission factors of different pollutants for the averaged cold-start UC cycle as well as different phases of the cycle. Figure S3: Time series of concentration of different pollutants (ppm) measured by FTIR in the first 150 s of the cold-start UC cycle. Figure S4: Time series of particle mass concentration and number concentration measured from CVS tunnel. Figure S5: Distribution of ultrafine particle mass emission factor and ultrafine particle number emission factor from the tested vehicle running on different fuels. Figure S6: Typical concentration profiles (ppb) during atmospheric aging. (PDF)

Department of Civil and Environmental Engineering, University of California – Davis, Davis, California 95616, United States

Abstract

Biogas consisting primarily of methane (CH_4) and carbon dioxide (CO_2) can be upgraded to a transportation fuel referred to as renewable natural gas (RNG) by removing CO_2 and other impurities. RNG has energy content comparable to fossil compressed natural gas (CNG) but with lower life-cycle greenhouse gas (GHG) emissions. In this study, a light-duty cargo van was tested with CNG and two RNG blends on a chassis dynamometer in order to compare the toxicity of the resulting exhaust. Tests for reactive oxygen species (ROS), biomarker expressions (CYP1A1, IL8, COX-2), and mutagenicity (Ames) show that RNG exhaust has toxicity that is comparable or lower than CNG exhaust. Statistical analysis reveals associations between toxicity and tailpipe emissions of benzene, dibenzofuran, and dihydroperoxide dimethyl hexane (the last identification is considered tentative/uncertain). Further gas-phase toxicity may be associated with tailpipe emissions of formaldehyde, dimethyl sulfide, propene, and methyl ketene. CNG exhaust contained higher concentrations of these potentially toxic chemical constituents than RNG exhaust in all of the current tests. Photochemical aging of the vehicle exhaust did not alter these trends. These preliminary results suggest that RNG adoption may be a useful strategy to reduce the carbon intensity of transportation fuels without increasing the toxicity of the vehicle exhaust.

Graphical Abstract

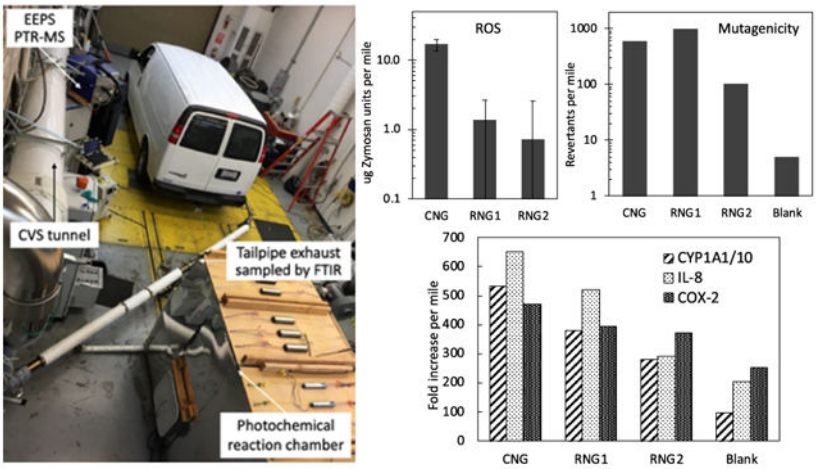

Keywords

Biomethane; CNG; RNG; Vehicle emissions; Toxicity

1. INTRODUCTION

Biogas produced from anaerobic digestion of organic waste is a useful renewable fuel that has lower lifecycle greenhouse gas (GHG) emissions than fossil fuels.[1,2] Raw biogas is typically only used for heat and power generation at the local production site because it has a

low methane (CH_4) content (50%–75%) and high carbon dioxide (CO_2) share (25%–50%). Upgraded biogas that removes CO_2 and other trace chemicals (hydrogen sulfide, halocarbons, siloxanes) can be used as a replacement fuel for traditional fossil natural gas in most applications. In California, biogas that has been upgraded to more than 89% methane[3] can be used as a transportation fuel commonly referred to as renewable natural gas (RNG) that can help reduce "well-to-wheels" GHG emissions by more than 50%[4] compared to fossil compressed natural gas (CNG).

A careful analysis of potential environmental and human health impacts should be conducted before widespread adoption of any new fuel, including RNG. Subramanian et al.[5] compared RNG and CNG vehicle emissions, finding slightly lower fuel economy and higher emissions of carbon monoxide (CO), hydrocarbons (HCs), and oxides of nitrogen (NOx) emissions from a RNG vehicle. Lim et al.[6] found that total hydrocarbons (THCs) in vehicle exhaust increase with increasing fuel CH_4 content, while exhaust polycyclic aromatic hydrocarbons (PAHs) and NOx increase with increasing concentration of higher hydrocarbons (ethane, propane) in the fuel. The relationship between fuel and exhaust composition has also been studied by modifying CNG composition.[7–11] Exhaust HCs were found to be correlated with fuel composition, and exhaust NO_X, CO, and PM were related to the technology used in the vehicle engine and exhaust control system. A few previous studies also measured CNG vehicle exhaust toxicity with bacterial mutagenicity tests and concluded that PM-induced toxicity response can be attributed to lubricating oil emissions and nitro-PAHs in the exhaust.[12–15] No previous study has examined exhaust toxicity from RNG-fueled vehicles.

In this study, exhaust emissions from a light-duty cargo van operating on commercial CNG and two RNG blends was analyzed for regulated compounds (CO_2, CO, NOx, N_2O, CH_4, HCs), particulate matter (PM), and a variety of unregulated compounds (alcohols, aldehydes, ketone, organic acids, aromatics). Exhaust was photochemically aged in a smog chamber to understand how chemical properties would evolve in the atmosphere. Exhaust toxicity was characterized with three different bioassays, and the pollutant contributions to toxicity were evaluated with elastic net regression combined with predictions from a mutagenicity model (VEGA-QSAR). Results from this study help inform scientists and regulators about the potential air quality and public health impacts of widespread adoption of RNG as a transportation fuel.

2. METHODS

2.1. RNG Sample Collection and Analysis.

RNG was collected from three different biogas facilities (two food waste digesters and one dairy waste digester) using a mobile membrane separation unit (model HL-X1, Helee Inc., Hayward, CA) as described in previous studies.[16,17] RNG was compressed to 3600 psi in 61 L cylinders (CNG Cylinders International, Oxnard, CA) using a natural gas compressor designed for refueling CNG vehicles (PHILL Compressor, BRC Fuel Maker Corporation; Cherasco, Italy). Each cylinder required ~10 h to fill using the small compressor, and 2–3 cylinders were filled at each site depending on the availability of RNG. The collected gas therefore represents the average composition of RNG over 2–3 days.

The fuel cylinder in the test vehicle maintained a minimum gas pressure of 1000 psi during normal operation. This resulted in fuel blending when the tank was refilled (~1/3 old fuel and ~2/3 new fuel). Note that fuel blending would frequently occur in real-world practice when vehicles switch between different CNG and RNG fueling stations depending on location. Table 1 lists the chemical compositions of the three different gaseous fuel blends tested in the current study. The first was commercial CNG from a commercial filling station (3528 E Foothill Blvd, Pasadena, CA). The second, named RNG1, was a mixture of 27.8% CNG and 72.2% RNG from a food waste digester. The third, named RNG2, was a mixture of 7.7% CNG, 33.5% RNG from dairy waste, 34.4% RNG from a food waste digester, and 24.4% RNG from a second food digester. Tables S6–S8 in the Supporting Information also list the chemical composition of each biomethane stream.

2.2. Vehicle Exhaust Collection and Chemical Analysis.

Motor vehicle exhaust tests were performed at the California Air Resources Board (CARB) Haagen-Smit Laboratory located in El Monte, CA. The lab is equipped with a 48-in. (1.2 m) single-roll electric chassis dynamometer for light-duty vehicles, a constant volume sampler (CVS, AVL CVS i60 medium-duty) operating at 22.3 $m^3 \cdot min^{-1}$, and an exhaust sampling system that meets certification requirements defined by 40 CFR 86. A 2015 Chevrolet Express 2500 cargo van designed to run on CNG was used for all emissions tests. This vehicle had a sequential fuel injection (SFI) system and a heated oxygen sensor (HO_2S) three way catalytic converter (TWC). No modifications were made to the vehicle when fueled with RNG. The standard California unified cycle (UC cycle) was selected as the driving schedule for all tests. The UC cycle consists of three phases: a “cold start” phase (Phase I: 300 s), a “stabilized phase” (Phase II: 1135 s), a “hot soak” period where the engine is off (600 s), and a final “hot start” phase (Phase III: 300 s, a repeat of phase I). A speed-time trace for the UC cycle is presented in Figure S1. The test vehicle was driven at a constant speed of 80 $km \cdot hr^{-1}$ for 5 min, and then stored in a room at a controlled temperature of 25 °C for 14 h prior to each cold-start test. Two tests were conducted for each fuel over a total of 6 days in the order of CNG, RNG1, and RNG2.

The concentrations of regulated gaseous constituents (CO, CO_2, NO_X, N_2O, CH_4, THC) were measured with a HORIBA MEXA-ONE motor exhaust gas analyzer platform (HORIBA, Ltd.). Diluted exhaust from each phase of the driving cycle was drawn at constant flow rate from the CVS tunnel into a Tedlar bag. Each phase-averaged bag was analyzed separately at the end of the driving cycle. Fourier-transform infrared spectroscopy (FTIR, AVL, SESAM 4) was used to measure a variety of gaseous species (CO_2, CO, NOx, NH_3, SO_2, small HCs) from the undiluted tailpipe exhaust. The FTIR measured at 1 Hz with a flow rate of 13 LPM through a heated (191 °C) sampling line to avoid interference from condensing water. A PTR-MS (Ionicon PTR-TOF 8000) measured a variety of volatile organic compounds (m/z 1~500) from the CVS tunnel at a rate of 1 Hz. A further sample gas dilution of 1:4 was applied for all of the tests to optimize the linear signal response range for the current condition. Limits of detection (LODs) were calculated as the average value of the background (measured before or after each test) plus 3 times the standard deviation. The LODs, listed in Tables S1 and S2, vary from 0.36 to 4.05 ppm for FTIR measurements and 0.5–38 ppb for PTR-MS measurements. An EEPS (TSI Model 3090) measured particles

with diameters between 6.4 and 523 nm from the CVS tunnel at a rate of 1 Hz. Exhaust from CVS was also collected with XAD-2 sorbent tubes (8 mm × 110 mm 400 mg/200 mg, SKC, Inc.) at a flow rate of 1 L min^{-1} throughout the UC cycle. The XAD-2 tubes were analyzed for semivolatile organic compounds (SVOCs) using an Agilent 7890B gas chromatograph followed by a 7200B quadrupole-time-of-flight mass spectrometer (GC-QTOF-MS). Details of the sorbent tube analysis are provided in the Supporting Information.

2.3. Vehicle Exhaust Toxicological analysis.

2.3.1. ROS Assay.—The macrophage reactive oxygen species (ROS) assay measures the ROS-generating capacity of exhaust PM samples collected on Teflon filters (47 mm, pore size 2 μm) and extracted in water. PM samples were collected at a flow rate of 61 LPM from the diluted CVS tunnel while the engine was running (1735 s total). Exhaust from two cold-start driving cycles with the same fuel were combined onto the same filter to collect sufficient material for analysis (a similar approach was used for all toxicity tests). Filters were sealed in cassettes and sent to the Wisconsin State Laboratory of Hygiene for ROS analysis, following the method described in previous studies.[18–20] Results are reported as an increase of fluorescence in treated samples relative to untreated controls. Further details are provided in the Supporting Information, and a summary of PM mass collected for different toxicity assays is presented in Figure S9.

2.3.2. Mutagenicity Assay.—The microsuspension modification of the Salmonella/microsome (Ames) assay described in previous studies[21,22] was used to measure the mutagenicity of exhaust PM. Samples were drawn at a flow rate of 225 LPM from the diluted CVS tunnel through 1 in. (2.54 cm) insulated stainless-steel tubing to a 90 mm precleaned Teflon filter (Zefluor, Pall, Ann Arbor, MI., 2 um pore size) in a stainless-steel filter holder. Filters were stored at −20 °C until shipment to the University of California, Davis, where they were extracted using pressurized dichloromethane (Burdick and Jackson GC grade) at 2000 psi and 100 °C. The extracts were then dried and redissolved in dimethyl sulfoxide (DMSO) for testing. Further details are provided in the Supporting Information.

2.3.3. Biomarker Assay.—The expression of in vitro pro-inflammatory markers induced by exhaust PM was measured in human U937 macrophage cells (American Tissue Culture Collection, Manassas, VA) following the methods described in a previous study.[23] Extracts were in dimethyl sulfoxide (DMSO). Measured biomarkers included Cytochrome P450 monooxygenase (CYP1A1) which is a marker for PAHs, Interleukin 8 (IL-8) which is a marker for inflammation, and Cyclooxygenase (COX-2) which is a key enzyme for production of prostaglandins mediating pain and inflammation. Further details are provided in the Supporting Information.

2.3.4. Elastic Net Regression.—Elastic net regression[24] was used to find relationships between the measured chemical features and toxicity responses. Toxicity data and chemical data (emission factors or mass spec peak area count) were $\log_2$ transformed, and chemical data was further cyclic loess normalized. The linear combination of chemical features that was most predictive of $\log_2$ transformed toxicity response was then identified by the elastic net regression. Positive coefficients were returned for each toxicity end point, with the larger

coefficients interpreted as a stronger association. A detailed description of the method is provided in the Supporting Information.

2.3.5. VEGA-QSAR Mutagenicity Model.—The VEGA-QSAR (quantitative structure activity relationship) model can be used to link chemical structures described by molecular descriptors to toxicity.[25] The mutagenicity (Ames test) of gas-phase species in the current study was predicted on a scale of 0–1 using the CONSENSUS model, v1.0.3. The concentrations of all gas-phase compounds quantified with PTR-MS were multiplied by their predicted mutagenicity score so that aggregate gas-phase mutagenicity totals could be calculated for each fuel (CNG, RNG1, or RNG2).

2.4. Photochemical Aging of Exhaust.

Photochemical aging experiments were conducted in a 5.5 m^3 Teflon chamber (0.051 mm NORTON FEP fluoropolymer film) equipped with UV light panels (50 $W \cdot m^{-2}$). The Teflon reaction chamber was flushed three times before each test with air that was precleaned using granulated activated carbon to remove background gases followed by a high efficiency particulate air (HEPA) filter to remove PM. Dark aging tests started by filling the reaction chamber to 33% capacity with precleaned air, followed by injecting freshly diluted exhaust from the CVS tunnel through a 0.5 in. (1.27 cm) insulated stainless steel transfer line at a constant flow rate of 60 LPM over the entire UC cycle while the engine was running (1735 s). The reaction chamber was then quickly filled to 100% capacity with precleaned air, yielding a well-mixed system. The reaction chamber was aged for 3 h to represent a typical photochemical cycle, while concentration changes were recorded by the PTR-MS that sampled at a flow rate of 0.05 LPM. The light aging tests followed the same experimental protocol except that 100 L of VOC surrogate gas (1.125 ± 0.022 ppmv *m*-xylene and 3.29 ± 0.07 ppmv *n*-hexane in air, Scott Marrin, Inc.) was injected into the chamber immediately after injecting the exhaust, creating a final VOC concentration of 90 ppbv. Hydroxyl radical concentrations during the light aging tests were calculated to be 5–6 × 10^6 molecules·cm^{-3} based on the decay rate of the *m*-xylene. The final ozone concentrations at the end of the 3 h experiment were measured to be 110–125 ppb.

3. RESULTS AND DISCUSSION

3.1. Fuel Composition.

Table 1 summarizes the concentrations of major and trace components in different fuels as well as basic fuel properties such as higher heating value (HHV) and stoichiometric air-fuel (A/F) ratio. Trace compound concentrations in each fuel are summarized in Tables S3–S5. CNG had the lowest CH_4 concentration but much higher ethane and propane concentration compared to the RNGs. RNG1 had more ethane and propane than RNG2 but similar CH_4 due to blending. Hence, the overall heating value and stoichiometric A/F ratio ranked CNG > RNG1 > RNG2. CO_2 increased as more RNG was blended into the fuel (CNG < RNG1 < RNG2) due to residual CO_2 in the RNG even after upgrading.

3.2. Exhaust Composition.

3.2.1. Gas-Phase Pollutant Emissions.

3.2.1.1. Regulated Pollutants and Fuel Economy.: Emission factors for regulated pollutants and fuel economies measured during the cold-start UC cycle are displayed in Figure S2, while the pollutant concentrations measured as a function of time by FTIR during the cold start period (first 150 s) are presented in Figure S3. The fuel economy of the test vehicle was highest when using CNG (2.87 miles·m^{-3}) with reduced fuel economy measured for RNG1 (−3.1%) and RNG2 (−4.9%). CO_2 emissions factors were inversely correlated with fuel economy, with the lowest values measured when using CNG (682 g·$mile^{-1}$) and slightly higher values measured for RNG1 (+1.2%) and RNG2 (+5.0%). Emissions of CO and total hydrocarbons (HCs) were +59% and +72% higher when using RNG2 relative to CNG, respectively, while emissions of nitrogen compounds (NO_X, N_2O, NH_3) were not strongly related to fuel composition. Further details of regulated pollutant emissions are provided in the Supporting Information.

3.2.1.2. Unregulated Gaseous Pollutants.: Figure 1(a–x) presents the emission factors of various VOCs and SVOCs measured by PTR-MS. For CNG and RNG1, only one set of measurements was considered valid and reported. CVS tunnel background concentrations were monitored before each test, and the averaged background values (bkg) were reported as part of the test measurements. Background (equivalent) emission factors account for the majority of the measured concentrations for many compounds, emphasizing the low emissions from both CNG and RNG combustion. The tunnel background concentrations observed in the current study are similar to those reported in previous studies.[12,26] More advanced measurement techniques, improved exhaust-sampling protocols, and new system designs will be required to measure low levels of tailpipe emissions in future vehicle tests involving clean fuels. In the present study, tailpipe emissions above background were detected by the PTR-MS in at least one test phase for formaldehyde, methanol, ethanol, propanol, dimethyl sulfide, propene, butene, methyl ketene, and benzene.

Figure 1a–d shows the emission factors for one aldehyde (formaldehyde) and three alcohols (methanol, ethanol, and propanol) that were emitted above background concentrations. These compounds are formed from the oxidation reactions in the combustion chamber, in the exhaust system, and on the surface of the three-way catalytic converter (TWC).[27–29] Studies have shown that the emission of these oxygenated compounds are primarily affected by the details of the combustion system with less impact from fuel composition especially for the smaller compounds (C_1, C_2—alcohols, aldehydes, ketones, acids), which can be formed through multiple reaction pathways. Important factors include the equivalent A/F ratio, exhaust oxygen and HC levels, and exhaust temperature and residence time. Zervas et al.[30,31] reported that emissions of small alcohols peaked at $\lambda = 1$ (stoichiometric conditions). Also, organic acid emissions increased when $\lambda > 1$ (lean burn conditions), and CO emissions increased when $\lambda < 1$ (rich burn conditions). Therefore, the observed different emissions rates for oxygenated HCs between CNG and RNGs as shown in Figure 1(a–d) are likely affected by the different combustion conditions, indirectly linking to fuel H/C ratios.

Emission factors for benzene (the only aromatic compound above background in the PTR-MS data) are presented in Figure 1(u). Benzene emissions from the different fuels were similar, with slightly higher emissions from vehicles fueled with CNG compared to RNG. Benzene emission factors measured in the current study are also similar in magnitude to those measured from previous tests on CNG and RNG vehicles.[6,32] Figure 1(k) shows that emissions of dimethyl sulfide (DMS) were higher in Phase 3 (hot catalyst) vs Phase 1 (cold catalyst). Previous studies have shown that sulfides can form on the surface of the hot catalyst with excess unburned fuel.[33] Emissions of propene (Figure 1(m)) and butene (Figure 1(n)) were similar when using CNG and RNG. Butene was emitted across all phases of the UC cycle, while propene was emitted mainly during the cold start (Phase 1).

Alignment of the nontarget GC-QTOF-MS data across different tests isolated 826 molecular features having similar retention indexes and primary mass spectral features. After applying filters to remove features with a maximum abundance in the samples less than five times the average tunnel blank and features with average signal-to-noise ratios below 10, a total of 74 features remained. Of these, 42 compounds were tentatively identified against the NIST17 mass spectral database, producing combined spectral similarity and retention index match scores above 800. A full list of these 42 compound abundances in the tailpipe exhaust is available in Table S10. A subset of 17/42 compounds were on our target list and are considered to be confirmed identifications including a number of substituted benzenes, substituted phenols, and polycyclic aromatic hydrocarbons. The remaining compounds are a diverse set that includes cycloalkanes (e.g., cyclohexane, 1-ethyl-1-methyl-), aldehydes/ketones (e.g., 3-furaldehyde), and heterocyclic aromatics (e.g,. 2-methylquinoline and 1,2-benzoisothiazole).

3.2.2. Particulate Matter Emissions.—Figure 2 presents ultrafine particle mass and number emission factors from the overall UC cycle. Tailpipe particulate matter number emissions were more than an order of magnitude higher than background concentrations. The CNG tests emitted a lower particle count but higher particle mass than the RNG tests, possibly because the CNG contained higher concentrations of C2 and C3 alkanes (ethane, propane) enhancing PM precursor formation.[6,9] PM precursors nucleate to form nanoparticles that grow and ultimately serve as condensation sites for lubricating oil that enters the combustion chamber. Multiple studies have shown that engine lubricating oil is a significant source of vehicle PM emissions[9,34–36] and that the level of oil emission, although not directly related to fuel composition, is closely related to the air/fuel ratio and combustion chamber temperature.[37] The higher heating value of the CNG may therefore influence the PM trends measured in the current study.

3.3. Atmospheric Aging of Exhaust.

Dilution and photochemical reactions will change the properties of the exhaust over time in the atmosphere. Figure S6 shows the time evolution of xylene and ethenone concentrations measured after dilution in a photochemical aging chamber using PTR-MS. Concentrations for both of these compounds were stable in 3 h dark aging tests (Figure S6(a, c)), but xylene injected at the beginning of the test was consumed while ethenone was formed during photochemical reactions in 3 h light aging tests (Figure S6(b, d)). Figure 3 presents final

concentrations of different chemical compounds measured at the end of 3 h aging experiments across multiple fuels. Butene concentrations were only slightly lower in light aging tests relative to dark tests, likely because butene is an intermediate breakdown product from surrogate VOC (hexane and xylene) reactions. The rest of the compounds summarized in Figure 3 were all oxygenated and increased in light aging tests. Most importantly in the context of the current study, engine exhaust from CNG and RNG behaved similarly during photochemical aging, suggesting similar atmospheric reaction pathways and products.

3.4. Exhaust Toxicity.

Figure 4(a–c) shows toxicity induced by engine exhaust PM measured using different bioassays. Figure 4(a) shows that the reactive oxygen species (ROS) present in the water-soluble portion of the PM is significantly higher in CNG exhaust compared to the exhaust from RNGs even when accounting for the variability of the three replicate analyses. Figure 4(b) shows the levels of biomarker expression (CYP1A1, IL-8, and COX-2, respectively) as fold-increased emissions above blank levels in U937 human macrophages. PM from CNG exhaust induced the highest biomarker signal followed by RNG1 and RNG2. The significant enhancement of ROS as well as higher level of pro-inflammation biomarkers from CNG exhaust were consistent with the higher PM mass emissions factor from CNG exhaust. Lubricating oil emissions have been reported to be strongly associated with ROS activity.[38] In contrast, the mutagenicity of CNG and RNG exhaust was similar (same order of magnitude), as shown in Figure 4(c). The mutagenicity measured in the CVS tunnel background was several orders of magnitude lower than the samples.

PM toxicity may be influenced by semivolatile chemical constituents that partition from the gas phase to the particle phase. The sorbent tubes used for the GC-QTOF-MS analysis in the current study capture gas-phase constituents and some fraction of the particle-phase constituents. These GC-QTOF-MS measurements complement the PTR-MS measurements discussed in the previous section. Elastic net regression was used to study the relationship between toxicity responses and chemical constituents measured by GC-QTOF-MS and PTR-MS (Figure 5). A total of 22 features with positive coefficients were selected by the regularized linear regression out of a list of 107 constituents. Chemical compounds that were strongly correlated with various toxicity responses include a subset of the small carbonyls (C1, C2—aldehydes, ketene) and many of the aromatic compounds. Naphthalene was measured with both PTR-MS and GC-QTOF-MS but in different units. Elastic net regression returned similar coefficients for the parallel naphthalene measurements, building confidence in the robustness of the results. Note that some of the significant chemical components identified in the elastic net regression analysis (including naphthalene) are primarily derived from the test background conditions (Figure 1).

Figure 6 summarizes all of the chemical components associated with toxicity in the current study using either emissions factor (μg·mile^{-1}) or emissions peak area depending on the measurement technique. Background concentrations (hatched patterns in Figure 6) account for the majority of the concentration for many of the species identified as toxicologically significant by elastic net regression. The background concentrations for the GC-QTOF-MS measurements were characterized with a single blank test, and so, the threshold for

significant tailpipe emissions was interpreted conservatively as three times the background level for these constituents. On the basis of the data in Figure 6, the primary tailpipe emissions associated with toxicity in the vehicle exhaust include benzene, dibenzofuran, and dihydroperoxide dimethyl hexane (the last identification is considered tentative/uncertain). In all cases, RNG tailpipe emissions of these potentially toxic compounds are lower than in CNG tailpipe emissions.

Elastic net regression was not able to detect associations between gas-phase chemical constituents and mutagenicity outcomes in the current study. The aggregated mutagenicity of the gas-phase exhaust was therefore calculated using the consensus Ames score from the VEGA-QSAR model for each tested fuel (Figure 7). The chemical constituents emitting above background levels in at least one phase of testing (Figure 1) that made the greatest contribution to gas-phase mutagenicity included formaldehyde, dimethyl sulfide, propene, and methyl ketene. Formaldehyde accounted for more than half of the aggregated exhaust mutagenic score for all of the fuels due to its abundance and toxicity. Gas-phase CNG exhaust had a higher aggregate mutagenic score compared to gas-phase RNG exhaust.

4. IMPLICATIONS

The results of the current study indicate that the toxicity of the exhaust from motor vehicles powered by RNG is less than or equal to the toxicity of the exhaust from vehicles powered by CNG. Photochemical aging of the exhaust had the same effect for CNG and RNG and therefore is not expected to alter this conclusion. Multiple studies show that modern CNG engines equipped with three-way catalysts (TWCs) operating under stoichiometric conditions emit far less pollution than older engines powered by CNG or diesel with a lean burn and oxidation catalyst (or even no aftertreatment). The corresponding toxicity of the exhaust from modern CNG engines is orders of magnitude lower than the toxicity of exhaust from older engines.[12,15,26,39] The widespread adoption of modern engines powered by RNG in the transportation sector to replace existing CNG or diesel engines should therefore yield reduced toxicity. Future studies should expand the testing to include a greater number of RNG fuels, more repetitions of the driving cycle, a broader range of medium-duty and heavy-duty vehicles, and an expanded suite of toxicology tests to confirm that the results from this preliminary study can be extended to the entire motor vehicle fleet.

Multiple studies have explored the technological and economic aspects of biogas upgrading under different biomethane production and utilization scenarios. The results indicate that the economic uncertainties in biogas production are substantial. Most studies agree that the scale of the biogas production plant, type of feedstock, and availability of tax incentives/subsidies are the most important economic factors.[40–44] Despite this economic uncertainty, the adoption of RNG to replace fossil fuels in the transportation sector appears to be a worthy policy goal since this fuel switch has the potential to further decarbonize energy production, yielding long-term climate benefits that complement the potential immediate public health benefits associated with reduced toxicity.

Supplementary Material

Refer to Web version on PubMed Central for supplementary material.

ACKNOWLEDGMENTS

The authors would like to thank the California Air Resources Board (CARB) (Project #13-418 & Project#17-ISD004) and the California Energy Commission (CEC) (Project #500-13-006) for funding this study. Christoph Vogel was supported by the National Institute of Environmental Health Sciences of the National Institutes of Health (NIH) under Award Number R01 ES029126. The statements and conclusions expressed in this paper do not necessarily reflect the views of the CARB, CEC, NIH, or University of California Davis, and no official endorsement should be inferred. The authors greatly appreciate cooperation and assistance from the CARB HAAGEN-SMIT Laboratory. Special thanks are due to Tin Truong, Aiko Matsunaga, Hyun-Ji Lee, Bruce Frodin, Henry Toutoundjian, Manuel Cruz, Thomas Valencia, Wayne McMahon, Mang Zhang, Richard Ling, and the dedicated staff in the Organic Analysis Section and Aerosol Analysis and Methods Evaluation Section. We thank Martin Shafer from the University of Wisconsin laboratory for ROS analyses. The authors also thank all the biogas/RNG producers who collaborated with this study. The authors thank Xiguang Chen and Helee LLC for their in-kind support through the provision of the membrane separation unit used to upgrade biogas to RNG.

REFERENCES

(1). Poeschl M; Ward S; Owende P Environmental Impacts of Biogas Deployment - Part I: Life Cycle Inventory for Evaluation of Production Process Emissions to Air. J. Cleaner Prod 2012, 24, 168–183.

(2). Poeschl M; Ward S; Owende P Environmental Impacts of Biogas Deployment - Part II: Life Cycle Assessment of Multiple Production and Utilization Pathways. J. Cleaner Prod 2012, 24, 184–201.

(3). Williams RB; Kaffka SR; Oglesby R Draft Interim Project Draft Report: Comparative Assessment of Technology Options for Biogas Clean-Up; California Energy Commission, 2014.

(4). Lyng KA; Brekke A Environmental Life Cycle Assessment of Biogas as a Fuel for Transport Compared with Alternative Fuels. Energies 2019, 12 (3), 532.

(5). Subramanian KA; Mathad VC; Vijay VK; Subbarao PMV Comparative Evaluation of Emission and Fuel Economy of an Automotive Spark Ignition Vehicle Fuelled with Methane Enriched Biogas and CNG Using Chassis Dynamometer. Appl. Energy 2013, 105 (x), 17–29.

(6). Lim C; Kim D; Song C; Kim J; Han J; Cha JS Performance and Emission Characteristics of a Vehicle Fueled with Enriched Biogas and Natural Gases. Appl. Energy 2015, 139 (2015), 17–29.

(7). Matthews R; Chiu J; Hilden D CNG Compositions in Texas and the Effects of Composition on Emissions, Fuel Economy, and Driveability of NGVs. SAE Tech. Pap. Ser 1996, 105 (May), 2170–2185.

(8). Karavalakis G; Durbin TD; Villela M; Miller JW Air Pollutant Emissions of Light-Duty Vehicles Operating on Various Natural Gas Compositions. J. Nat. Gas Sci. Eng 2012, 4, 8–16.

(9). Hajbabaei M; Karavalakis G; Johnson KC; Lee L; Durbin TD Impact of Natural Gas Fuel Composition on Criteria, Toxic, and Particle Emissions from Transit Buses Equipped with Lean Burn and Stoichiometric Engines. Energy 2013, 62, 425–434.

(10). Kakaee AH; Paykani A; Ghajar M The Influence of Fuel Composition on the Combustion and Emission Characteristics of Natural Gas Fueled Engines. Renewable Sustainable Energy Rev. 2014, 38, 64–78.

(11). Park C; Kim C; Lee S; Lee S; Lee J Comparative Evaluation of Performance and Emissions of CNG Engine for Heavy-Duty Vehicles Fueled with Various Caloric Natural Gases. Energy 2019, 174, 1.

(12). Kado NY; Okamoto RA; Kuzmicky PA; Kobayashi R; Ayala A; Gebel ME; Rieger PL; Maddox C; Zafonte L Emissions of Toxic Pollutants from Compressed Natural Gas and Low Sulfur Diesel-Fueled Heavy-Duty Transit Buses Tested over Multiple Driving Cycles. Environ. Sci. Technol 2005, 39 (19), 7638–7649. [PubMed: 16245838]

(13). Seagrave JC; Gigliotti A; McDonald JD; Seilkop SK; Whitney KA; Zielinska B; Mauderly JL Composition, Toxicity, and Mutagenicity of Particulate and Semivolatile Emissions from Heavy-

Duty Compressed Natural Gas-Powered Vehicles. Toxicol. Sci 2005, 87 (1), 232–241. [PubMed: 15976195]

(14). Turrio-Baldassarri L; Battistelli CL; Conti L; Crebelli R; De Berardis B; Iamiceli AL; Gambino M; Iannaccone S Evaluation of Emission Toxicity of Urban Bus Engines: Compressed Natural Gas and Comparison with Liquid Fuels. Sci. Total Environ 2006, 355 (1–3), 64–77. [PubMed: 16442433]

(15). Yoon S; Hu S; Kado NY; Thiruvengadam A; Collins JF; Gautam M; Herner JD; Ayala A Chemical and Toxicological Properties of Emissions from CNG Transit Buses Equipped with Three-Way Catalysts Compared to Lean-Burn Engines and Oxidation Catalyst Technologies. Atmos. Environ 2014, 83 (X), 220–228.

(16). Li Y; Alaimo CP; Kim M; Kado NY; Peppers J; Xue J; Wan C; Green PG; Zhang R; Jenkins BM; Vogel CFA; Wuertz S; Young TM; Kleeman MJ Composition and Toxicity of Biogas Produced from Different Feedstocks in California. Environ. Sci. Technol 2019, 53, 11569. [PubMed: 31479247]

(17). Peppers J; Li Y; Xue J; Chen X; Alaimo C; Wong L; Young T; Green PG; Jenkins B; Zhang R; Kleeman MJ Performance Analysis of Membrane Separation for Upgrading Biogas to Biomethane at Small Scale Production Sites. Biomass Bioenergy 2019, 128, 105314.

(18). Landreman AP; Shafer MM; Hemming JC; Hannigan MP; Schauer JJ A Macrophage-Based Method for the Assessment of the Reactive Oxygen Species (ROS) Activity of Atmospheric Particulate Matter (PM) and Application to Routine (Daily-24 h) Aerosol Monitoring Studies. Aerosol Sci. Technol 2008, 42 (11), 946–957.

(19). Shafer MM; Perkins DA; Antkiewicz DS; Stone EA; Quraishi TA; Schauer JJ Reactive Oxygen Species Activity and Chemical Speciation of Size-Fractionated Atmospheric Particulate Matter from Lahore, Pakistan: An Important Role for Transition Metals. J. Environ. Monit 2010, 12 (3), 704–715. [PubMed: 20445860]

(20). Wang D; Pakbin P; Shafer MM; Antkiewicz D; Schauer JJ; Sioutas C Macrophage Reactive Oxygen Species Activity of Water-Soluble and Water-Insoluble Fractions of Ambient Coarse, PM2.5 and Ultrafine Particulate Matter (PM) in Los Angeles. Atmos. Environ 2013, 77, 301–310.

(21). Kado NY; Langley D; Eisenstadt E A Simple Modification of the Salmonella Liquid-Incubation Assay Increased Sensitivity for Detecting Mutagens in Human Urine. Mutat. Res. Lett 1983, 121 (1), 25–32.

(22). Kado NY; Guirguis GN; Flessel CP; Chan RC; Chang K-I; Wesolowski JJ Mutagenicity of Fine Airborne Particles: Diurnal Variation in Community Air Determined by a Salmonella Micro Preincubation (Microsuspension) Procedure. Environ. Mutagen 1986, 8 (1), 53–66. [PubMed: 3510862]

(23). Vogel CFA; Garcia J; Wu D; Mitchell DC; Zhang Y; Kado NY; Wong P; Trujillo DA; Lollies A; Bennet D; Schenker MB; Mitloehner FM Activation of Inflammatory Responses in Human U937 Macrophages by Particulate Matter Collected from Dairy Farms: An in Vitro Expression Analysis of pro-Inflammatory Markers. Environ. Health 2012, 11 (1), 1–9. [PubMed: 22236490]

(24). Zou H; Hastie T Regularization and Variable Selection via the Elastic Net. J. R. Stat. Soc. Ser. B Stat. Methodol 2005, 67 (5), 768.

(25). Benfenati E; Manganaro A; Gini G VEGA-QSAR: AI inside a Platform for Predictive Toxicology. In CEUR Workshop Proceedings, 2nd Workshop on Popularize Artificial Intelligence, PAI 2013, Turin, Italy, 2013; Vol. 1107, pp 21–28.

(26). Okamoto RA; Kado NY; Kuzmicky PA; Ayala A; Kobayashi R Unregulated Emissions from Compressed Natural Gas (CNG) Transit Buses Configured with and without Oxidation Catalyst. Environ. Sci. Technol 2006, 40 (1), 332–341. [PubMed: 16433369]

(27). Wagner T; Wyszynski ML Aldehydes and Ketones in Engine Exhaust Emissions—A Review. Proc. Inst. Mech. Eng., Part D 1996, 210 (2), 109–122.

(28). Nichols RJ; Clinton EL; King ET; Smith CS; Wineland RJ A View of Flexible Fuel Vehicle Aldehyde Emissions. SAE Tech. Pap. Ser 1988, 97 (May), 422–429.

(29). Nakamura H; Motoyama H; Kiyota Y Passenger Car Engines for the 21st Century; SAE Technical Paper 911908; SAE International, 1991. DOI: 10.4271/911908.

(30). Zervas E; Montagne X; Lahaye J C1 – C5 Organic Acid Emissions from an SI Engine: Influence of Fuel and Air/Fuel Equivalence Ratio. Environ. Sci. Technol 2001, 35 (13), 2746–2751. [PubMed: 11452603]

(31). Zervas E; Montagne X; Lahaye J Emission of Alcohols and Carbonyl Compounds from a Spark Ignition Engine. Influence of Fuel and Air/Fuel Equivalence Ratio. Environ. Sci. Technol 2002, 36 (11), 2414–2421. [PubMed: 12075798]

(32). Shah A; Yun-shan G A Comparative Study on VOCs and Aldehyde-Ketone Emissions from a Spark Ignition Vehicle Fuelled on Compressed Natural Gas and Gasoline. Pak. J. Eng. Appl. Sci 2012, 10, 29–35.

(33). Cadle SH; Mulawa PA Sulfide Emissions from Catalyst-Equipped Cars. SAE Tech. Pap. Ser 1978, na DOI: 10.4271/780200.

(34). Thiruvengadam A; Besch MC; Yoon S; Collins J; Kappanna H; Carder DK; Ayala A; Herner J; Gautam M Characterization of Particulate Matter Emissions from a Current Technology Natural Gas Engine. Environ. Sci. Technol 2014, 48 (14), 8235–8242. [PubMed: 24960475]

(35). Jayaratne ER; He C; Ristovski ZD; Morawska L; Johnson GR A Comparative Investigation of Ultrafine Particle Number and Mass Emissions from a Fleet of On-Road Diesel and CNG Buses. Environ. Sci. Technol 2008, 42 (17), 6736–6742. [PubMed: 18800557]

(36). Kuwayama T; Collier S; Forestieri S; Brady JM; Bertram TH; Cappa CD; Zhang Q; Kleeman MJ Volatility of Primary Organic Aerosol Emitted from Light Duty Gasoline Vehicles. Environ. Sci. Technol 2015, 49 (3), 1569–1577. [PubMed: 25493342]

(37). Gautam M; Thiruvengadam A; Carder D; Besch M; Shade B; Thompson G; Clark N Testing of Volatile and Nonvolatile Emissions from Advanced Technology Natural Gas Vehicles; Final Report Contract No. 07–340, California Air Resources Board, Sacramento CA.

(38). Cheung KL; Ntziachristos L; Tzamkiozis T; Schauer JJ; Samaras Z; Moore KF; Sioutas C Emissions of Particulate Trace Elements, Metals and Organic Species from Gasoline, Diesel, and Biodiesel Passenger Vehicles and Their Relation to Oxidative Potential. Aerosol Sci. Technol 2010, 44 (7), 500–513.

(39). Yoon S; Collins J; Thiruvengadam A; Gautam M; Herner J; Ayala A Criteria Pollutant and Greenhouse Gas Emissions from CNG Transit Buses Equipped with Three-Way Catalysts Compared to Lean-Burn Engines and Oxidation Catalyst Technologies. J. Air Waste Manage. Assoc 2013, 63 (8), 926–933.

(40). Von Wald G; Brandt A; Rajagopal D; Stanion A; Sweeney JL; Mace AJ; Brady SE Biomethane in California Common Carrier Pipelines: Assessing Heating Value and Maximum Siloxane Specifications; California Council on Science & Technology, 2018.

(41). Pääkkönen A; Aro K; Aalto P; Konttinen J; Kojo M The Potential of Biomethane in Replacing Fossil Fuels in Heavy Transport-a Case Study on Finland. Sustainability 2019, 11 (17), 4750.

(42). Rotunno P; Lanzini A; Leone P Energy and Economic Analysis of a Water Scrubbing Based Biogas Upgrading Process for Biomethane Injection into the Gas Grid or Use as Transportation Fuel. Renewable Energy 2017, 102, 417–432.

(43). Cucchiella F; D'Adamo I Technical and Economic Analysis of Biomethane: A Focus on the Role of Subsidies. Energy Convers. Manage 2016, 119, 338–351.

(44). Cucchiella F; D'Adamo I; Gastaldi M Biomethane: A Renewable Resource as Vehicle Fuel. Resources 2017, 6 (4), 58.

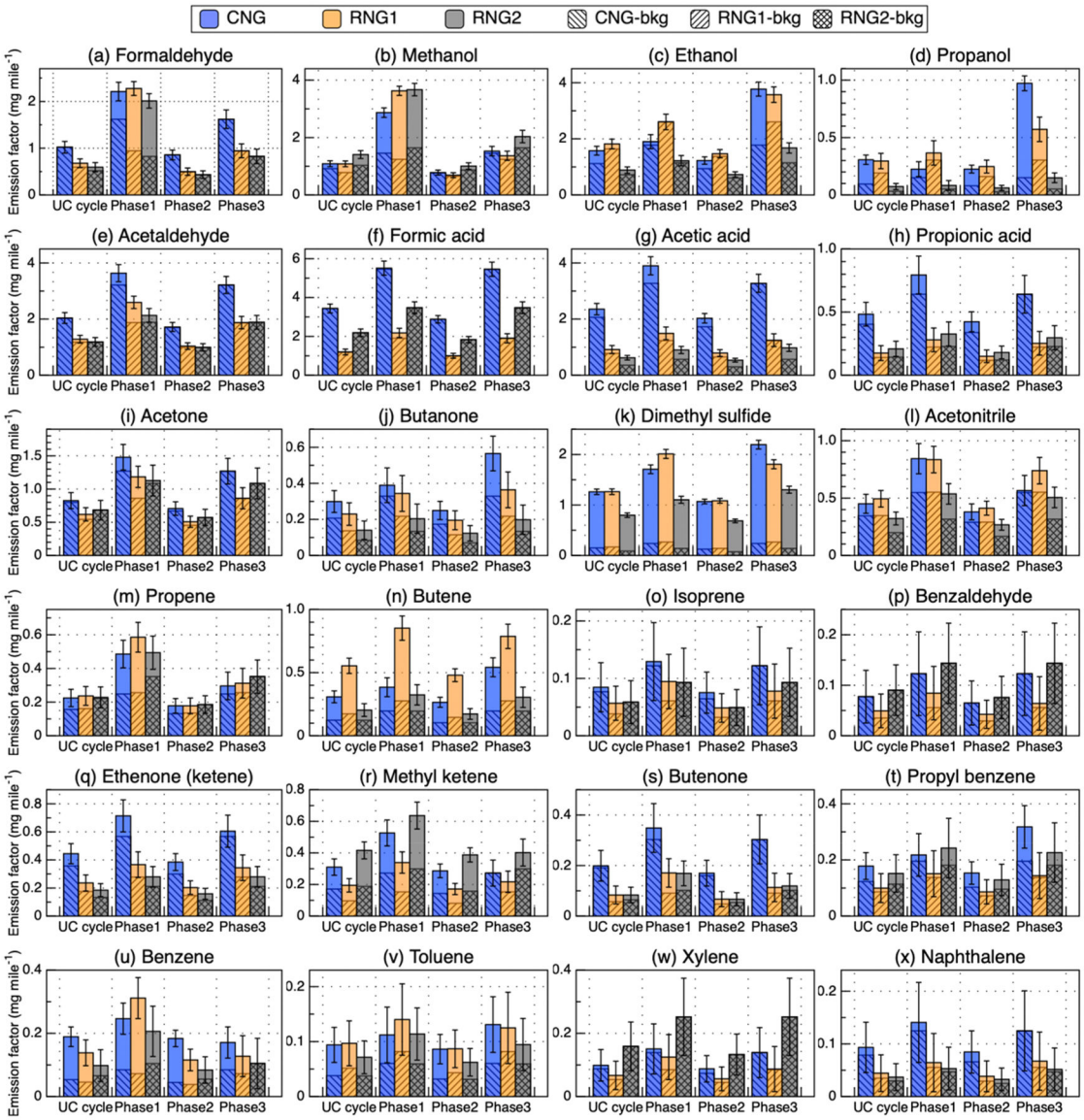

Figure 1.

(a–x) Emission factors (mg·mile^{-1}) of different pollutants for the averaged cold-start UC cycle as well as different phases of the cycle. Error bar represents standard deviation of the tunnel background measurement.

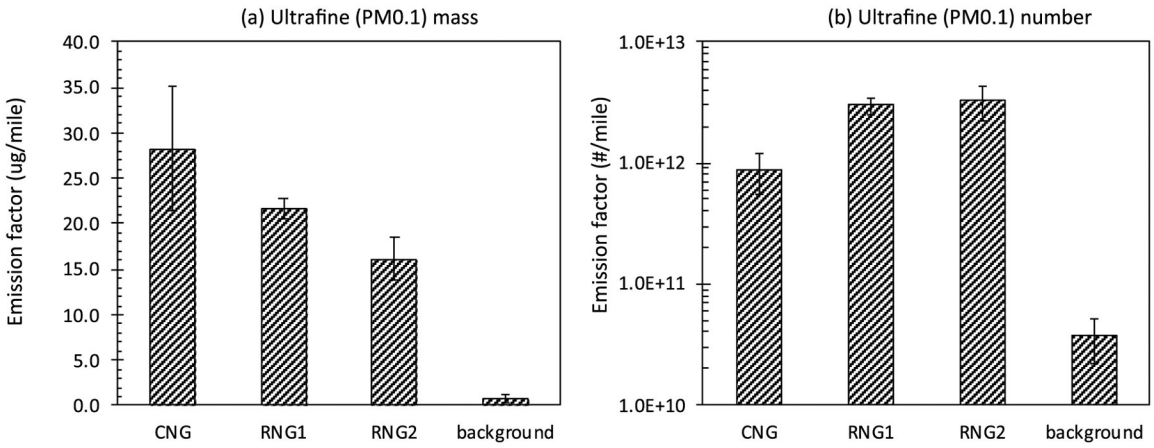

Figure 2.

UC cycle-averaged emission factor of ultrafine particle ($PM_{0.1}$): (a) mass ($\mu g \cdot mile^{-1}$) and (b) number ($\#\cdot mile^{-1}$) from the tested vehicle running on different fuels. The height of the bars represents the average value of total PM mass or number emission factor calculated from EEPS measurement (only including 6.4–93.1 nm) of the duplicate tests on the same fuel. Error bars represent the min and max values from the duplicate tests on the same fuel.

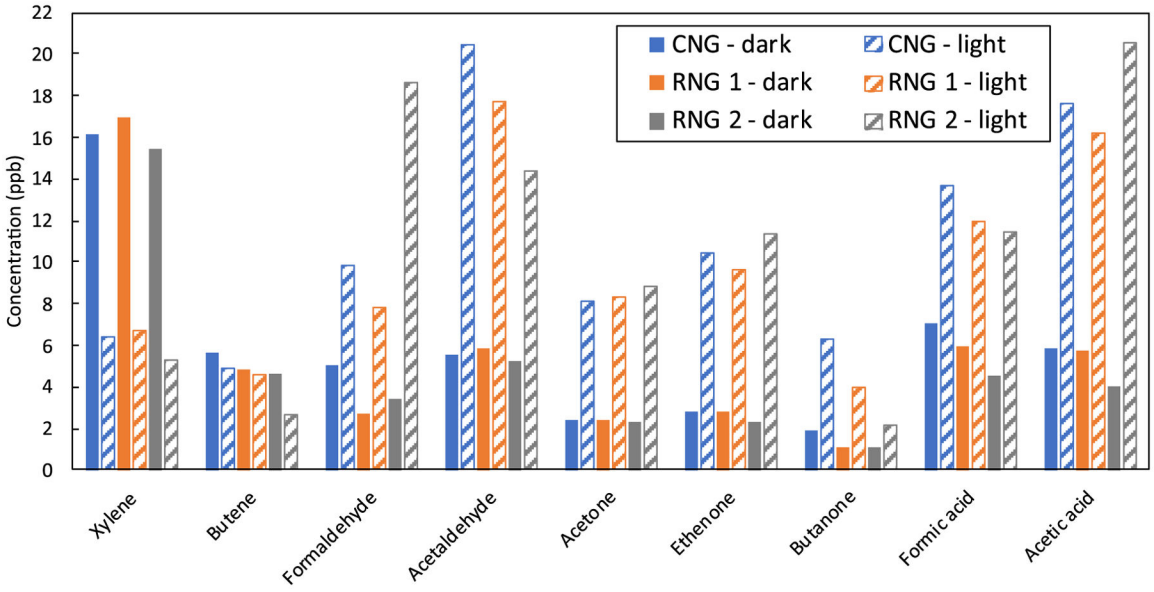

Figure 3.

Concentration (ppb) of selected compounds measured from chamber after 3 h of aging under either a dark or light condition.

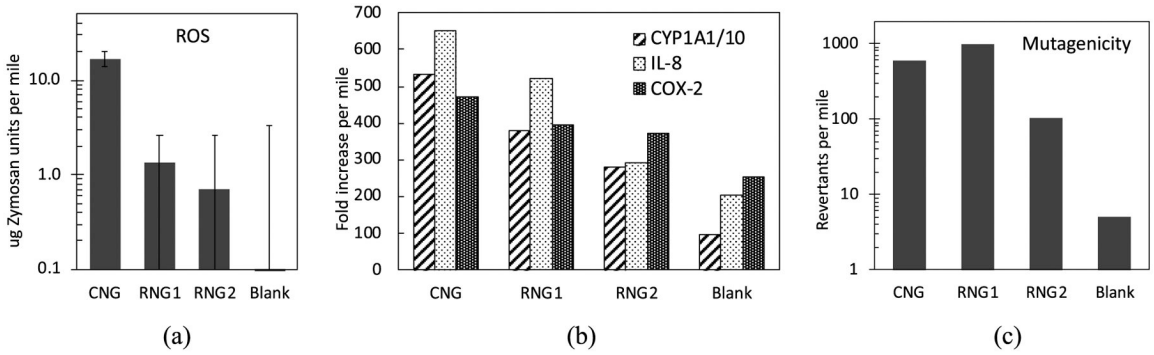

Figure 4.

Toxicity of vehicle exhaust running on different fuels: (a) reactive oxygen species (ROS) measured with macrophage assay (error bars represent the standard deviation resulting from three replicate analysis of the same sample), (b) pro-inflammatory biomarker expression measured in human U937 macrophage cells (CYP1A1 is divided by 10 and plotted), and (c) mutagenicity measured with a microsuspension modification of the Salmonella/microsome (AMES) assay.

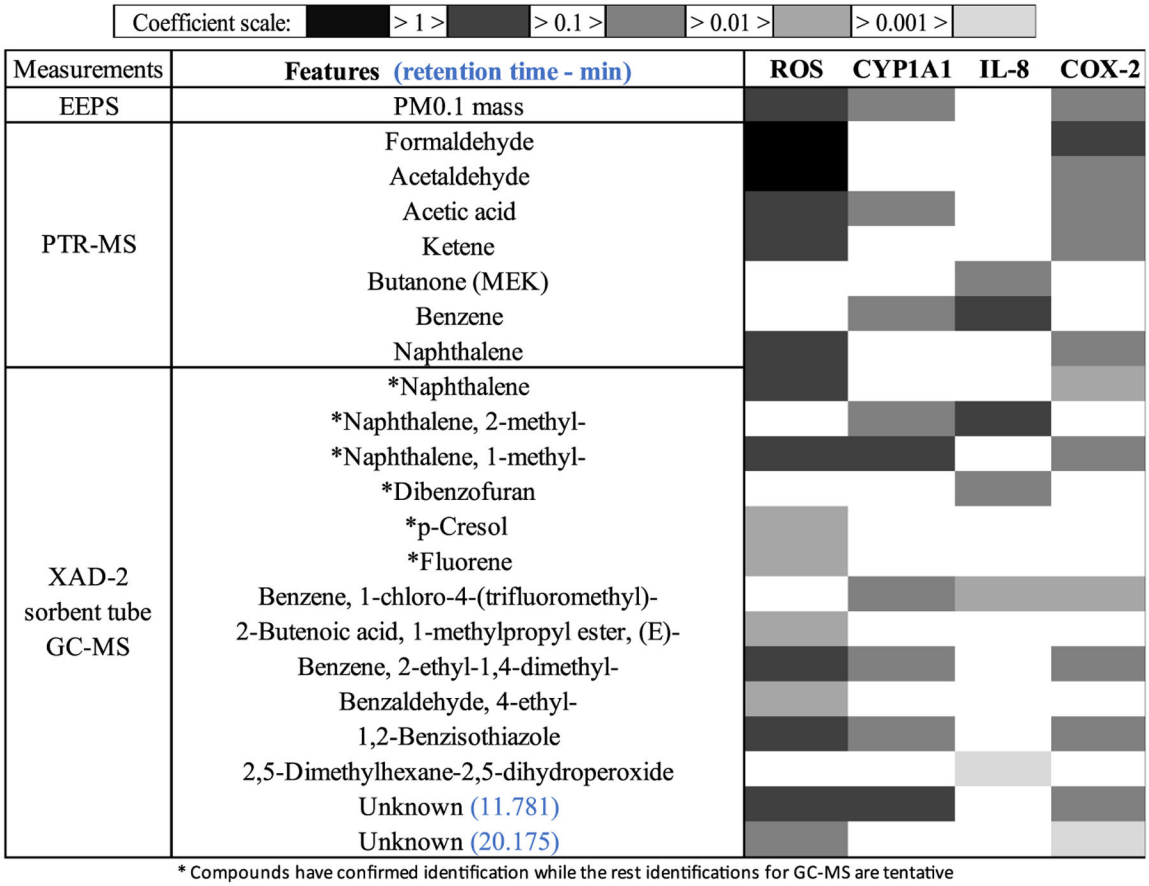

Figure 5.

Summary of elastic net regression results on the linear coefficients between chemical features and toxicity responses.

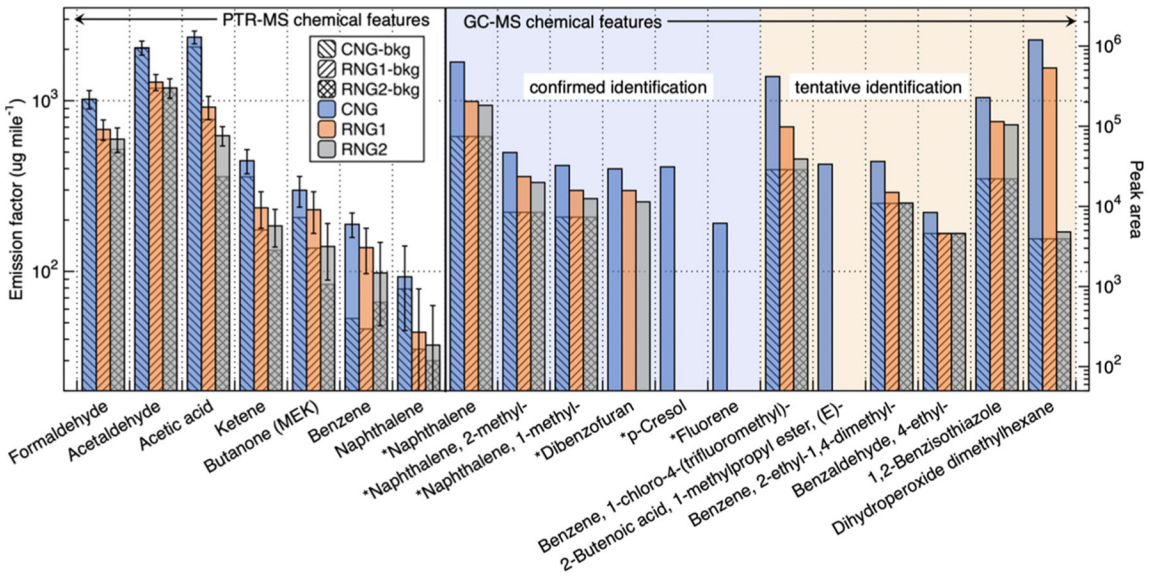

Figure 6.

Abundance of selected chemical compounds that had a nonzero coefficient associated with toxicity responses (units in ug·mile^{-1} for PTR-MS measurements and peak area for XAD + GC-QTOF-MS measurements). Background signals shown for PTR-MS were measured before each test with error bars representing standard deviations of the background measurements. Background signals shown for GC-QTOF-MS were measured with a dedicated tunnel blank sorbent tube sample.

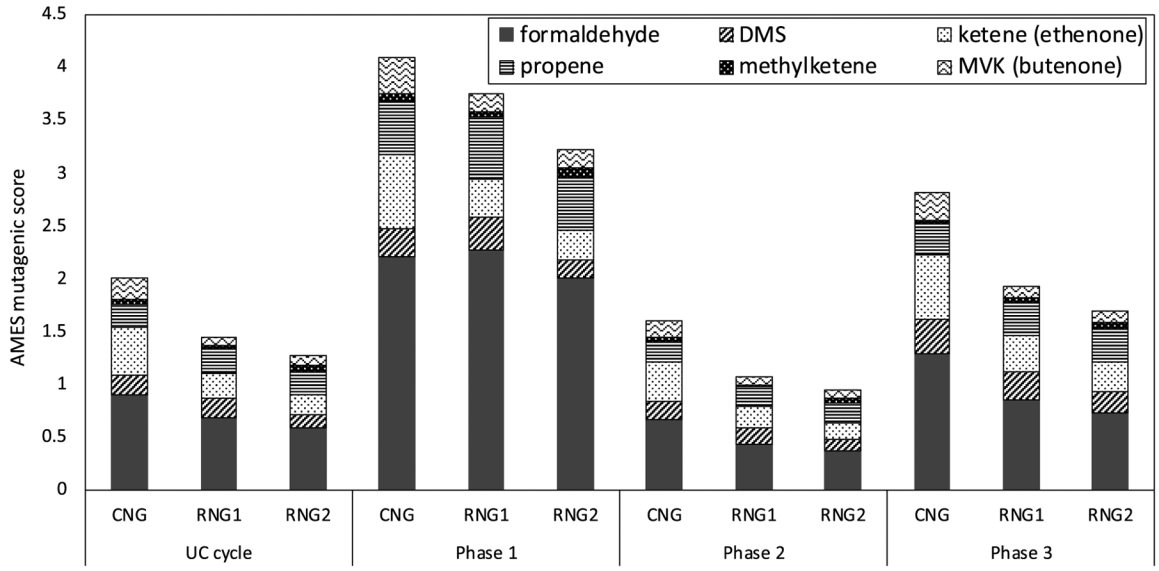

Figure 7.

Mutagenic score calculated based on gas-phase concentration measured by PTR-MS and AMES test consensus score given by the VEGA-QSAR model.

Table 1.

Compositions of Different Fuels Used in This Study[a]

Compound	unit	CNG	RNG 1	RNG 2
Methane	%	91.2% ± 0.8%	93.5% ± 1.3%	93.3% ± 0.6%
Ethane	%	5.41% ± 0.18%	1.50% ± 0.05%	0.42% ± 0.01%
Propane	%	0.33% ± 0.06%	0.09% ± 0.02%	0.03% ± 0.00%
Carbon dioxide	%	0.82% ± 0.09%	1.85% ± 0.39%	4.28% ± 0.18%
Nitrogen	%	1.83% ± 0.65%	2.64% ± 1.01%	1.77% ± 0.48%
Oxygen	%	0.42% ± 0.30%	0.42% ± 0.11%	0.18% ± 0.04%
Aromatic hydrocarbons	ppm	1.84 ± 0.24	1.73 ± 0.07	1.27 ± 0.12
Other hydrocarbons	ppm	7.04 ± 0.59	9.44 ± 2.23	5.11 ± 1.07
Sulfur-containing compounds	ppm	1.11 ± 0.18	1.95 ± 0.55	1.96 ± 0.36
Higher heating value	$MJ \cdot m^{-3}$	38.27 ± 0.34	36.31 ± 0.47	35.46 ± 0.22
Stoichiometric air/fuel ratio	kg/kg	16.21 ± 0.15	15.67 ± 0.22	14.94 ± 0.10

[a]Concentration of methane, ethane, propane, carbon dioxide, nitrogen, and oxygen are reported in percentage (with 1 standard deviation). Concentration of different hydrocarbons and sulfur-containing compounds are reported in ppm by volume (with 1 standard deviation). Fuel higher heating value and stoichiometric air/fuel ratios are calculated based on the measured major compounds (%) listed in this table.